Altering lipid droplet homeostasis affects *Coxiella burnetii* intracellular growth

Minal Mulye[1], Brianne Zapata[1,2], and Stacey D. Gilk[1*]

[1] Department of Microbiology and Immunology, Indiana University School of Medicine, Indianapolis, Indiana, United States of America.

[2] Department of Biology, California State University, Dominguez Hills, Carson, California, United States of America.

*Corresponding author: 635 Barnhill Rd, MS 420, Indianapolis, IN 46202. Telephone: 317-274-8028. Fax: 317-278-3331. E-mail: sgilk@iupui.edu

Running title: Lipid droplets during *Coxiella burnetii* infection.

ABSTRACT

Coxiella burnetii is an obligate intracellular bacterial pathogen and a causative agent of culture-negative endocarditis. While *C. burnetii* initially infects alveolar macrophages, it was also found in lipid droplet (LD)-containing foamy macrophages in the cardiac valves of endocarditis patients. In addition, transcriptional studies of *C. burnetii*-infected macrophages reported differential regulation of the LD coat protein-encoding gene perilipin 2 *(plin-2)*. To further investigate the relationship between LDs and *C. burnetii*, we compared LD numbers in mock-infected and *C. burnetii*-infected alveolar macrophages using fluorescence microscopy. Compared to only 10% of mock-infected cells, 50% of *C. burnetii*-infected cells had more than 50 LDs/cell as early as 24 hours post-infection, indicating a significant increase in LDs in infected cells. Increased LDs required the *C. burnetii* Type 4B Secretion System (T4BSS), a major virulence factor that manipulates host cellular processes by secreting bacterial effector proteins into the host cell cytoplasm. To determine the importance of LDs during *C. burnetii* infection, we assessed the effect of manipulating LD homeostasis on *C. burnetii* intracellular growth. Surprisingly, blocking LD formation with the pharmacological inhibitors triascin C or T863, or knocking out acyl-CoA transferase-1 *(acat-1)* in alveolar macrophages, increased *C. burnetii* growth at least 2-fold. Conversely, preventing LD lipolysis by inhibiting adipose triglyceride lipase (ATGL) with atglistatin almost completely blocked bacterial growth, suggesting LD breakdown is essential for *C. burnetii*. Together these data suggest that LDs are detrimental to *C. burnetii* and maintenance of LD homeostasis, possibly via the T4BSS, is critical for bacterial growth.

IMPORTANCE

Host neutral lipid storage organelles known as lipid droplets (LDs) serve as a source of energy, nutrients, or signaling lipids during infection with intracellular bacteria, such as *Mycobacterium* spp., and *Chlamydia* spp. LDs have also been associated with infection of the intracellular bacterial pathogen *Coxiella burnetii*, a significant cause of culture-negative infectious endocarditis. Although *C. burnetii* was found in LD-rich foam macrophages in endocarditis patients, little is known about the host LD-*C. burnetii* relationship. We demonstrated a *C. burnetii* Type 4B Secretion System (T4BSS)-dependent LD accumulation in macrophages, suggesting that the T4BSS plays a key role in regulating host cell LD formation or breakdown. Further, manipulation of LD homeostasis significantly affected *C. burnetii* intracellular growth, indicating LDs play an important role during *C. burnetii* infection. Since *C. burnetii* endocarditis has a 19% mortality rate even in treated patients, exploring the LD-*C. burnetii* association might identify novel therapeutic targets.

INTRODUCTION

Lipid droplets (LDs) are dynamic cytoplasmic organelles which store cellular lipids in eukaryotic cells. LDs are uniquely comprised of a phospholipid monolayer surrounding a hydrophobic core of neutral lipids, primarily sterol esters and triacylglycerols. LD assembly begins with neutral lipid synthesis, where fatty acyl CoA synthetases generate long chain fatty acids which are converted to sterol esters and triacyglycerols by acyl-CoA:cholesterol acyltransferase (ACAT) and acyl-CoA:diacylglycerol acyltransferase (DGAT), respectively. Progressive accumulation of neutral lipids in the ER leads to budding of the lipid ester globule, surrounded by the ER membrane cytoplasmic leaflet (1, 2). Hormone sensitive lipase (HSL) (3)

and adipose triglyceride lipase (ATGL) (4) mediate LD breakdown and release of free cholesterol and fatty acids. Functionally, LDs serve as intracellular lipid reservoirs for membrane synthesis or energy metabolism. In addition, LDs are linked to a range of cellular functions including protein storage, protein degradation and signaling (2, 5).

LDs are emerging as important players during host-pathogen interactions. During infection of host cells, Hepatitis C virus (HCV) (6) and Dengue virus (7) co-opt LDs as platforms for viral assembly and replication. Even though pharmacological manipulation of LD content reduced viral numbers, the importance of LDs during viral infection still remains elusive (8). Increased LD numbers in host cells is observed upon infection with several pathogens including HCV (6) and Dengue virus (7), as well as the protozoan parasites *Trypanosoma cruzi* (9), *Plasmodium berghei* (10), *Toxoplasma gondii* (11), *Leishmania amazonensis* (12) and *Leishmania major* (13). In addition, the intracellular bacterial pathogens *Chlamydia* spp. (14), *Mycobacterium* spp. (15-18), *Orientia tsutugamushi* (19), and *Salmonella typhimurium* (20) also increase LD numbers in infected cells. *C. trachomatis (14, 21)* and *M. tuberculosis* (15) are thought to use triacylglycerol and cholesterol esters stored in LDs as a major source of energy and nutrients. Furthermore, in cells infected with *M. leprae* (22), *M. bovis* (16), *T. cruzi* (23), and *Leishmania infantum chagasi* (24), LDs serve as a source of prostaglandin and leukotriene eicosanoids, important signaling lipids which modulate inflammation and the immune response. These LD-derived eicosanoids potentially favor intracellular pathogen survival by downregulating the immune response (25).

LDs have been implicated during infection by *Coxiella burnetii*, a gram-negative intracellular bacterium and the causative agent of human Q fever. Primarily spread through aerosols, *C. burnetii* acute infection is characterized by a debilitating flu-like illness, while

chronic disease results in endocarditis. Although *in vitro* and *in vivo C. burnetii* can infect a wide range of cells including epithelial cells and fibroblasts, the bacterium first infects alveolar macrophages during natural infection. Inside the host cell, *C. burnetii* directs formation of a specialized lysosome-like compartment called the parasitophorous vacuole (PV) which is essential for *C. burnetii* survival. PV biogenesis requires the *C. burnetii* type 4B secretion system (T4BSS), which secretes effector proteins into the host cell cytoplasm where they manipulate a wide range of cellular processes. While not established to be T4BSS-dependent, *C. burnetii* is thought to manipulate LDs and other components of host cell lipid metabolism (26-29). *C. burnetii*-containing LD-filled foam cells were found in heart valves of an infected patient (30), and LDs were observed in the *C. burnetii* PV lumen of infected human alveolar macrophages (31). Further, two separate microarray analyses reported differential regulation of the LD coat protein *plin-2* in *C. burnetii*-infected human macrophage-like cells (THP-1) (28, 29), suggesting *C. burnetii* induced changes in host cell LDs. Intriguingly, siRNA depletion of the phospholipase involved in LD breakdown, PNPLA2 (also known as ATGL), increased the number of *C. burnetii* PVs in HeLa epithelial cells (32). In addition, treatment of monkey kidney epithelial cells (Vero cells) with a broad spectrum antiviral molecule ST699, which localizes to the host cell LDs, inhibited *C. burnetii* intracellular growth (33). Despite these observations, the importance of LDs during *C. burnetii* infection is not known. In this study, we further examined the relationship between host LDs and *C. burnetii*. We observed a T4BSS-dependent increase in LD numbers in infected alveolar and monocyte-derived macrophages. Furthermore, manipulation of LD homeostasis significantly altered *C. burnetii* intracellular growth, thus strongly indicating that LDs play an important role during *C. burnetii* infection.

RESULTS AND DISCUSSION

C. burnetii infection results in host cell LD accumulation.

To examine the role of LDs in *C. burnetii* pathogenesis, we first quantitated LDs in infected cells. Previously, two separate microarray studies reported differential regulation of the LD coat protein-encoding gene *plin-2* in *C. burnetii*-infected cells (28, 29), generally indicating changes in LD numbers. As *C. burnetii* preferentially infects alveolar macrophages during natural infection, we utilized a mouse alveolar macrophage cell line (MH-S) previously shown as a model for *C. burnetii* infection (34). Cells were stained by immunofluorescence for the LD coat protein PLIN2, and LD number per cell determine by fluorescence microscopy. During a 4-day mock infection, the majority of macrophages (~80%) had less than 50 LDs per cell, irrespective of the time point (Figure 1). In contrast, we observed a significant increase in LDs per cell at 1, 2 and 4 days after *C. burnetii* infection, with >60% of infected cells having more than 50 LDs. Notably, LD accumulation occurred as early as 1 day post-infection, when the PV has not expanded and the bacteria are not in log growth. This suggests that LD accumulation is not a host response to a large PV, but could be a result of *C. burnetii* directly manipulating host LDs.

Host cell LD accumulation is dependent on the *C. burnetii* Type 4B Secretion System (T4BSS).

Previously, based on microarray analysis of *C. burnetii*-infected cells where bacterial protein synthesis was blocked, Mahapatra *et al.* identified 36 host cell genes specifically regulated by *C. burnetii* during early stages of infection. These genes were predominantly involved in the innate immune response, cell death and proliferation, vesicular trafficking, cytoskeletal organization and lipid homeostasis. Interestingly, changes in *plin-2* expression level

in infected cells was dependent on *C. burnetii* protein synthesis (28). Together with our data, this suggests that *C. burnetii* actively manipulates host LDs as early as day 1 post-infection, possibly through *C. burnetii* T4BSS effector proteins secreted into the host cytoplasm. The *C. burnetii* T4BSS detectably secretes effector proteins beginning 1 hour post-infection in bone marrow-derived macrophages and 8 hours post-infection in HeLa cells (35). To test if the *C. burnetii* T4BSS was responsible for LD accumulation in murine alveolar macrophages, LD numbers were analyzed at 1, 2, and 4 days after infection with a T4BSS *dotA* mutant. While at least 75% of the wild-type *C. burnetii*-infected cells had >50 LDs at all time points, only 40% cells infected with T4BSS mutant had >50 LDs per cell, similar to mock-infected cells (Figure 2A and B). This suggests the T4BSS is involved in increased LDs in *C. burnetii*-infected alveolar macrophages.

To confirm this finding, we analyzed LD numbers in human macrophage-like cells (THP-1). Similar to murine alveolar macrophages, when compared to mock- or T4SS mutant-infected cells, wild-type *C. burnetii*-infected THP-1 cells had increased LD numbers at 1 and 4 days post-infection (Figure 2C). Interestingly, we did not observe T4BSS-dependent LD accumulation at 2 days post-infection. However, these results demonstrate that the *C. burnetii*-induced increase in LDs in both human and mouse macrophages is species-independent and dependent on the *C. burnetii* T4BSS.

The requirement for the *C. burnetii* T4BSS suggests that one or more *C. burnetii* T4BSS effector proteins may actively manipulate LDs. Other bacteria have been shown to target host LDs via effector proteins. For example, the *C. trachomatis* secreted protein Lda3 localizes to the LD surface and is involved in LD translocation into the *Chlamydia*-containing inclusion (21). The *Salmonella* Typhimurium type 3 secretion system (T3SS) effector protein SseJ esterifies cholesterol and increases LD numbers when expressed in epithelial and macrophage cells (20).

Thus far, none of the identified *C. burnetii* T4BSS secreted effector proteins localize to host LDs. While *C. burnetii* effectors might directly target proteins involved in LD formation or LDs themselves, it is also possible that fission of preexisting LDs, and not *de novo* formation, is responsible for increased numbers of LDs (36). As observed in Figure 2A, the LD size in *C. burnetii*-infected macrophages appeared smaller than the mock- or T4BSS mutant-infected macrophages. Smaller, more numerous LDs might result from *C. burnetii* T4BSS-mediated fission of the existing LDs.

While *C. burnetii* T4SS effector proteins might directly target LDs or LD pathways, LD accumulation may also be a host innate immune response. In other diseases, LD accumulation occurs during the inflammatory response in macrophages in atherosclerotic lesions (37), leukocytes from joints of patients with inflammatory arthritis (38), and eosinophils in allergic inflammation (39). Thus, an innate immune response to the T4BSS apparatus or T4BSS effector proteins may increase LD numbers in *C. burnetii*-infected macrophages. While our data demonstrate that the *C. burnetii* T4BSS is involved in LD accumulation in both mouse and human macrophages, the bacterial effector proteins and the specific LD processes involved remain unknown.

Blocking LD formation increases *C. burnetii* growth.

Given our finding that the *C. burnetii* T4BSS may manipulate host LD accumulation, we next assessed the importance of LDs during *C. burnetii* infection. We first blocked LD formation using triascin C, a long chain fatty acyl CoA synthetase inhibitor (40). Compared to vehicle control, triascin C significantly reduced macrophage LDs, with <5 LDs per cell (Figure 3A). We next treated macrophages with triascin C during *C. burnetii* infection, and quantitated bacterial

177 growth using a fluorescent infectious focus-forming unit (FFU) assay. At various times post-
178 infection, we recovered bacteria from MH-S cells, replated onto a monolayer of Vero cells, and
179 incubated for 5 days. After staining for *C. burnetii*, we counted the number of fluorescent foci,
180 with 1 focus equivalent to 1 viable bacterium. Surprisingly, compared to vehicle-treated cells,
181 triascin C treatment increased *C. burnetii* growth 5-fold at 4 days post-infection (Figure 3B).
182 To further validate these results, we used CRISPR/Cas-9 to knockout *acat-1* (Figure 3C),
183 the enzyme responsible for sterol esterification. While *acat-1*$^{-/-}$ LDs lack sterol esters,
184 fluorescence microscopy revealed similar LD numbers in wild-type and *acat-1*$^{-/-}$ cells (Figure
185 3D). Compared to wild-type cells, *C. burnetii* growth in *acat-1*$^{-/-}$ cells increased 2-fold at 4 days
186 post-infection (Figure 3E), indicating that blocking sterol esterification favors *C. burnetii*
187 growth. To further deplete both triacylglycerol-and sterol ester-containing LDs, we treated *acat-*
188 *1*$^{-/-}$ cells with the DGAT1 inhibitor T863, which specifically blocks formation of triacylglycerols
189 (41). T863 treatment significantly reduced LDs in *acat-1*$^{-/-}$ macrophages, compared to untreated
190 wild-type or *acat-1*$^{-/-}$ macrophages (Figure 3D). *C. burnetii* growth increased 2-fold in T863-
191 treated *acat-1*$^{-/-}$ cells compared to vehicle-treated *acat-1*$^{-/-}$ cells (Figure 3F), demonstrating that
192 blocking both sterol ester- and triacylglycerol-containing LDs improves *C. burnetii* growth.
193 These studies demonstrate that both pharmaceutical and genetic approaches to blocking
194 LD formation increases *C. burnetii* fitness in macrophages. Interestingly, Mahapatra *et al.*
195 observed an increase in *plin-2* transcript levels after transiently blocking *C. burnetii* protein
196 synthesis, suggesting that wild-type *C. burnetii* downregulates LD formation (28). It is not clear
197 why inhibiting LD formation is advantageous to *C. burnetii*. While it is not known if *C. burnetii*
198 uses host fatty acids, unesterified free fatty acids or sterols in LD-deficient cells may support *C.*
199 *burnetii* growth.

Inhibiting LD breakdown blocks *C. burnetii* growth.

Because blocking LD formation appeared to benefit *C. burnetii*, we next examined *C. burnetii* growth after inhibiting LD breakdown and increasing LD numbers. When cells or tissues need fatty acids or cholesterol, cytosolic lipases such as hormone sensitive lipase (HSL) (2, 3) and adipose triglyceride lipase (ATGL) (4) hydrolyze triacylglycerols and sterol esters stored in LDs. To block LD breakdown in murine macrophages, we inhibited ATGL with the selective and competitive inhibitor atglistatin, which binds the ATGL patatin-like phospholipase domain (42). To eliminate the possibility of ATGL inhibiting a *C. burnetii* phospholipase, we first measured viability of axenic *C. burnetii* cultures in the presence or absence of atglistatin (Figure 4A). Treatment for 4 days had no effect on axenic bacterial growth, indicating atglistatin does not directly affect *C. burnetii*.

We next tested the effect of atglistatin on intracellular bacteria. After atglistatin treatment of wild-type MH-S cells, we observed larger LDs by immunofluorescence microscopy, although the number did not significantly increase (Figure 3A). Interestingly, *C. burnetii* intracellular growth in atglistatin-treated wild-type MH-S cells decreased 5-fold, with essentially no growth (Figure 4B). Further, atglistatin-treated *acat-1*$^{-/-}$ cells, which contain triacylglycerol-containing LDs, also showed reduced bacterial growth (Figure 4C). Together, these data demonstrate that blocking LD breakdown significantly inhibits intracellular *C. burnetii* growth, regardless of LD composition.

Our data suggest that LD breakdown is essential for *C. burnetii* intracellular growth in macrophages. Previously, siRNA knockdown of ATGL in HeLa cells increased the number of *C. burnetii* PVs, although the effect on *C. burnetii* growth was not determined (32). LDs are less

abundant in HeLa cells compared to macrophages, and LDs and LD breakdown may play a larger role during *C. burnetii* infection of macrophages. LD breakdown liberates fatty acids, which can be reesterified or serve as signaling cofactors, building blocks for membranes, or substrates for β -oxidation to generate energy (2). Several intracellular bacteria use LD-derived fatty acids as a source of energy and carbon. *M. tuberculosis*, which can make its own LDs, converts host-derived fatty acids into triacylglycerol, which is then deposited in bacterial LDs (15). The *M. tuberculosis* lipase is hypothesized to release stored bacterial fatty acids, but can also degrade host LD-derived triacylglycerol (43). Host LDs translocated into the *C. trachomatis* inclusion may be broken down to provide lipids for bacterial growth (14). We did not observe LDs in the *C. burnetii* PV lumen in murine macrophages or THP-1 macrophage-like cells, in contrast to reports in human alveolar macrophages (31). It is not known if free fatty acids or sterols liberated from LDs, either in the cytosol or possibly the PV lumen, support *C. burnetii* growth.

In addition to serving as a source of free fatty acids and sterols, macrophage LDs are rich in substrates and enzymes that generate prostaglandins and leukotrienes, which are arachidonic acid-derived inflammatory lipid mediators (44, 45). In *M. leprae*-infected Schwann cells and *M. bovis* BCG-infected macrophages, increased LD biogenesis correlates with increased production of prostaglandin E2 (PGE2), linking LDs to the production of innate immunity modulators (17, 46). Thus, LDs can serve as a source of inflammatory mediators in response to pathogen infection. Interestingly, elevated levels of PGE2 were observed in *C. burnetii* endocarditis patients and linked to *C. burnetii*-mediated immunosuppression. Koster *et al.* reported lymphocytes from chronic Q fever patients being unresponsive to *C. burnetii* antigens, an effect reversed by PGE2 suppression with indomethacin (47). In addition, after stimulation with *C.*

246 *burnetii* antigens, monocytes from Q fever patients produced PGE2, which in turn
247 downregulated T lymphocyte-mediated IL-2 and IFNγ production. Interestingly, PGE2 synthesis
248 inhibitor Piroxicam reversed this downregulation of pro-inflammatory cytokine production (48).
249 Thus, while PGE2 appears to play a role in Q fever patients, the relationship between *C.*
250 *burnetii*-induced LDs and PGE2 production is not known. Considering that LD breakdown can
251 serve multiple functions, *C. burnetii* could use LDs either as a source of nutrients or for
252 production of lipid immune mediators like PGE2, which could then modulate the host cell
253 response to promote *C. burnetii* intracellular growth.

254 In summary, our data demonstrate that LD homeostasis is important for *C. burnetii*
255 intracellular survival. Because the *C. burnetii* T4BSS is involved in LD accumulation,
256 characterizing bacterial T4BSS effector proteins that target host LD homeostasis will help further
257 understand the role of LDs in *C. burnetii* pathogenesis.

258

259 **MATERIALS AND METHODS**

260 Bacteria and mammalian cells

261 *C. burnetii* Nine Mile Phase II (NMII; clone 4, RSA439) were purified from Vero cells (African
262 green monkey kidney epithelial cells, ATCC CCL-81; American Type Culture Collection,
263 Manassas, VA) and stored as previously described (49). For experiments examining T4BSS-
264 dependent accumulation of LDs, NMII and the *dotA* mutant (50) were grown for 4 days in
265 ACCM-2, washed twice with phosphate buffered saline (PBS) and stored as previously described
266 (51). Vero, mouse alveolar macrophages (MH-S; ATCC CRL-2019) and human monocytes
267 (THP-1; ATCC TIB-202) were maintained in RPMI (Roswell Park Memorial Institute) 1640
268 medium (Corning, New York, NY, USA) containing 10% fetal bovine serum (Atlanta

Biologicals, Norcross, GA, USA) at 37°C and 5% CO_2 and human embryonic kidney 293 (HEK293T; ATCC CRL-3216) in DMEM (Dulbecco's Modified Eagle Medium) (Corning, New York, NY, USA) containing 10% fetal bovine serum at 37°C and 5% CO_2. THP-1 cells were differentiated with 200 nM of phorbol 12-myristate 13-acetate (PMA) for 24 hours. PMA was removed, and the cells rested for 48 hours prior to infection. The multiplicity of infection (MOI) was optimized for each bacterial stock, cell type and infection condition for a final infection of ~1 internalized bacterium/cell at 37°C and 5% CO_2.

Generating *acat-1*$^{-/-}$ MH-S cell line

The guide RNA sequence 5′TCGCGTCTCCATGGCTGCCC3′ to mouse *acat-1* was selected using the optimized CRISPR design site crispr.mit.edu. Oligonucleotides were synthesized (IDT, Coralville, IA, USA), annealed, and cloned into the lentiCRISPRv2 plasmid (a gift from Feng Zhang, Addgene # 52961, Cambridge, MA, USA) (52), at the BsmBI restriction site to generate plentiCRISPRv2-*acat-1*. To generate lentivirus, HEK293T cells were co-transfected with plentiCRISPRv2-*acat-1* and packaging plasmids pVSVg (Addgene # 8454), pRSV-Rev (Addgene # 12253), and pMDLg/pRRE (Addgene # 12251) using FuGENE6 reagent (Promega, Madison, WI, USA). At 48 hours post-transfection, supernatant was collected and centrifuged at 3000xg, and then filtered with 0.45µm filter to remove cells and debris. Supernatant was concentrated using the Lenti-X concentrator (Catalog # PT4421-2, Clontech, USA) and viral RNA isolated using Viral RNA isolation kit (Catalog # 740956, Macherey-Nagel, Germany) to determine viral titer using Lenti-X qRT-PCR titration kit (Catalog # PT4006-2, Clontech). Viral titers were optimized for transduction of MH-S cells to generate stable *acat-1*$^{-/-}$ cells.

291 $2x10^5$ MH-S cells were plated in a 6 well plate and transduced with 5.8 x 10^6 viral
292 particles/ml. 1 µg/ml puromycin was used for selection 48 hours post-transduction and
293 continued for 24 hours. The puromycin was then removed and the cells allowed to recover
294 before isolating individual clones by limiting dilution.
295 To confirm disruption of *acat-1*, clones were lysed in 2% SDS (Sigma-Aldrich, St. Louis,
296 MO, USA) for SDS-PAGE and immunoblotting with 1:1000 rabbit anti-mouse ACAT1-specific
297 antibody (Catalog # NBP189285, Novus Biologicals, Littleton, CO, USA) and 1:4000 GAPDH
298 loading control monoclonal antibody (Catalog # MA5-15738, ThermoFisher Scientific,
299 Waltham, MA, USA). The multiplicity of infection (MOI) was optimized for each bacterial stock
300 for a final infection of ~1 internalized bacterium/cell.
301
302 LD quantitation
303 $1x10^5$ MH-S cells were plated onto ibidi-treated channel µslide $VI^{0.4}$ ($3x10^3$ cells per channel;
304 Ibidi, Verona, WI) and allowed to adhere overnight. After infecting with *C. burnetii* for 1 hour,
305 cells were gently washed with phosphate buffered saline (PBS) to remove extracellular bacteria,
306 and incubated in 10% FBS-RPMI. At different times post-infection, infected cells were fixed
307 with 2.5% paraformaldehyde on ice for 15 min, then permeabilized/blocked for 15 min with
308 0.1% saponin and 1% bovine serum albumin (BSA) in PBS (saponin-BSA-PBS) and stained
309 with 1:1000 rabbit anti-mouse PLIN2 primary antibody (Catalog # PA1-16972, ThermoFisher
310 Scientific), 1:2000 guinea-pig anti-*C. burnetii* primary antibody (53) and 1:1000 rat anti-LAMP
311 (Catalog # 553792, BD Biosciences) primary antibody in saponin-BSA-PBS for 1 hour. THP-1
312 cells were stained with 1:500 guinea-pig anti-human PLIN2 primary antibody (Catalog # 20R-
313 AP002, Fitzgerald Industries International, Acton, MA), 1:2000 rabbit anti-*C. burnetii* primary

antibody and 1:1000 rat anti-LAMP primary antibody in saponin-BSA-PBS for 1 hour. After three washes with PBS, cells were stained with 1:2000 AlexaFluor 488 anti-rabbit, AlexaFluor 594 anti-guinea pig and AlexaFluor 647 anti-rat secondary antibodies (Invitrogen) for 1 hour. ProLong Gold mount (Invitrogen) was added to the wells after washing with PBS and slides visualized on a Leica inverted DMI6000B microscope (100X oil). The number of LDs per cell was quantitated for 50 cells per condition in three individual experiments, with only bacteria-containing cells counted for *C. burnetii*-infected cells. Each experiment was done in duplicate.

Inhibitors

Each LD homeostasis inhibitor used was diluted in DMSO based on manufacturer's instructions and optimum inhibitor concentration was determined based on 100% host cell viability determined by trypan blue staining, and changes in LD numbers per cell. The optimum concentrations determined for each inhibitor was: Triascin C (Enzo Life Sciences, Farmingdale, NY, USA) – 10 µM, T863 (Sigma-Aldrich) – 10 µM, Atglistatin (Cayman Chemicals, Ann Arbor, MI, USA) – 20 µM.

C. burnetii growth by fluorescent infectious focus-forming unit (FFU) assay.

To measure growth of *C. burnetii* in wild-type and *acat-1*$^{-/-}$ MH-S cells, 5x10^4 cells/well were infected for 1 hour in a 48 well plate, washed with PBS, and then incubated with media containing respective vehicle and inhibitors. At the indicated time points, the media was removed and cells were incubated with sterile water for 5 min, pipetted up and down and the lysate diluted 1:5 in 2% FBS-RPMI. Serial dilutions were added to 24 well plate containing confluent monolayers of Vero cells, incubated for 5 days, fixed with methanol and stained with

rabbit anti-*C. burnetii* antibody as well as DAPI to confirm monolayer integrity. Four fields per well were captured on an Evos automated microscope (ThermoFisher) with 4X objective and fluorescent foci units were quantitated using ImageJ. Each experiment was done in duplicate.

Atglistatin-treatment of *C. burnetii* axenic cultures

To test bacterial sensitivity to atglistatin, ACCM-2 was inoculated at approximately $1x10^5$ bacteria/ml with *C. burnetii* NMII and grown for 3 days as previously described (51). Bacteria (500 µl) were then incubated with DMSO or atglistatin in 24 well plates under normal *C. burnetii* culture conditions. Media was replenished every 24 hours by centrifuging the supernatant at 20000xg for 10 min, and bacterial pellet resuspended in new media containing inhibitor. After 4 days, bacteria were diluted 1:10 in 2% FBS-RPMI and serial dilutions were added to confluent Vero cell monolayers in a 96 well ibidi-treated µplate. At 5 days post-infection, the plate was stained and fluorescent foci were determined as above. Each experiment was done in duplicate.

Statistical analysis

Statistical analyses were performed using ordinary one-way ANOVA or two-way ANOVA with Tukey's or Bonferroni's multiple comparisons test in Prism (GraphPad Software, Inc., La Jolla, CA).

FIGURE LEGENDS:

Figure 1: *C. burnetii* infection results in host cell LD accumulation.

MH-S macrophages were infected with *C. burnetii* NMII and at different times post-infection, cells were stained for PLIN2 (LDs), LAMP1 (PV marker) and *C. burnetii*. LDs were observed by fluorescence microscopy and number of LDs per cell was quantitated. The percent of counted cells containing 0-20, 21-50 and >50 LDs per cell at respective times were plotted. Error bars show the mean of 3 independent experiments +/- SEM * =$p<0.05$, ** =$p<0.01$, *** =$p<0.001$ compared to respective >50 LDs/cell in mock-infected cells as determined by two-way ANOVA with Tukey post-hoc test.

Figure 2: Host cell LD accumulation is dependent on the *C. burnetii* T4BSS Secretion System (T4BSS).

A) Representative images of mock, wild-type *C. burnetii* NMII and T4BSS *(dotA)* mutant-infected MH-S macrophages stained for PLIN2 (LDs) at day 1 post-infection imaged at 100X. Scale bar = 10 µm

B) MH-S macrophages and (C) THP-1 monocyte-derived macrophages were infected with wild-type *C. burnetii* NMII and *dotA* mutant. At different time points post-infection, cells were stained for PLIN2 (LDs), LAMP1 (PV marker) and *C. burnetii*. The number of LDs per cell were counted by fluorescence microscopy. Percent of cells containing 0-20, 21-50 and >50 LDs per cell at respective time points were plotted. Error bars show the mean of 3 independent experiments +/- SEM * =$p<0.05$ compared to respective >50 LDs/cell in *dotA* mutant-infected cells as determined by two-way ANOVA with Tukey post-hoc test.

Figure 3: Blocking LD formation increases *C. burnetii* growth.

C. burnetii NMII growth in infected MH-S cells treated with different inhibitors was measured at 2 and 4 days post-infection by FFU assay.

A) Representative images for wild-type MH-S macrophages treated with inhibitors, fixed, stained for PLIN2 (LDs) and imaged day 1 post-treatment at 100X. Scale bar = 10 µm

B) Growth in LD formation inhibitor triascin C–treated (10 µM) wild-type MH-S macrophages. Error bars represent the mean of 4 independent experiments +/- SEM. **= p <0.01 compared to vehicle treated cells as determined by two-way ANOVA with Bonferroni post-hoc test.

C) ACAT1 protein expression in wild-type and *acat-1*$^{-/-}$ macrophages. Cell lysates were immunoblotted and ACAT1 protein levels were compared with GAPDH as loading control.

D) Representative images for vehicle-treated wild-type MH-S macrophages and vehicle and T863-treated *acat-1*$^{-/-}$ macrophages fixed, stained for PLIN2 (LDs) and imaged day 1 post-treatment at 100X. Scale bar = 10 µm

E) *C. burnetii* NMII growth in vehicle-treated wild-type and *acat-1*$^{-/-}$ MH-S macrophages and (F) T863-treated wild-type and *acat-1*$^{-/-}$ MH-S macrophages. Error bars represent the mean of 3 independent experiments +/- SEM., * =p<0.05, *** =p <0.001 as determined by two-way ANOVA with Bonferroni post-hoc test.

Figure 4: Inhibiting LD breakdown blocks *C. burnetii* growth.

Effect of ATGL inhibitor atglistatin on viability of axenic and intracellular *C. burnetii* was determined by FFU assay.

A) Direct effect of atglistatin on *C. burnetii* NMII. Atglistatin was added to axenic *C. burnetii* NMII cultures and bacterial viability was determined at day 4 using FFU assay. Error bars

represent the mean of 3 independent experiments +/- SEM. ns = not significant compared to vehicle treatment as determined by ordinary one-way ANOVA with Tukey post-hoc test.

B) Growth in atglistatin-treated (20 µM) and vehicle-treated wild-type MH-S macrophages. Error bars represent the mean of 4 independent experiments +/- SEM. *= p <0.05, **** =p<0.0001 compared to vehicle-treated cells as determined by two-way ANOVA with Bonferroni post-hoc test.

C) Growth in atglistatin-treated (20 µM) and vehicle-treated *acat-1*$^{-/-}$ MH-S macrophages. Error bars represent the mean of 4 independent experiments +/- SEM. ** =p<0.01 compared to vehicle treated cells as determined by two-way ANOVA with Bonferroni post-hoc test.

ACKNOWLEDGMENTS

This research was supported by National Institutes of Health (5R21AI21786; S.D.G.), American Heart Association (16POST27250157; M.M.) and National Institutes of Health (5R25GM07592; B.Z.). We thank Anna Justis, Tatiana Clemente and Rajshekar Gaji for critical reading of the manuscript and members of the IU Biology of Intracellular Pathogens Group for helpful suggestions.

We have no conflicts of interest to declare.

REFERENCES

1. **Pol A, Gross SP, Parton RG.** 2014. Review: biogenesis of the multifunctional lipid droplet: lipids, proteins, and sites. The Journal of Cell Biology **204:**635-646.
2. **Walther TC, Farese RV, Jr.** 2012. Lipid droplets and cellular lipid metabolism. Annual Review of Biochemistry **81:**687-714.
3. **Vaughan M, Berger JE, Steinberg D.** 1964. Hormone-Sensitive Lipase and Monoglyceride Lipase Activities in Adipose Tissue. The Journal of Biological Chemistry **239:**401-409.

4. **Haemmerle G, Lass A, Zimmermann R, Gorkiewicz G, Meyer C, Rozman J, Heldmaier G, Maier R, Theussl C, Eder S, Kratky D, Wagner EF, Klingenspor M, Hoefler G, Zechner R.** 2006. Defective lipolysis and altered energy metabolism in mice lacking adipose triglyceride lipase. Science **312:**734-737.
5. **Welte MA.** 2007. Proteins under new management: lipid droplets deliver. Trends in Cell Biology **17:**363-369.
6. **Filipe A, McLauchlan J.** 2015. Hepatitis C virus and lipid droplets: finding a niche. Trends in Molecular Medicine **21:**34-42.
7. **Samsa MM, Mondotte JA, Iglesias NG, Assuncao-Miranda I, Barbosa-Lima G, Da Poian AT, Bozza PT, Gamarnik AV.** 2009. Dengue virus capsid protein usurps lipid droplets for viral particle formation. PLoS Pathogens **5:**e1000632.
8. **Herker E, Ott M.** 2012. Emerging role of lipid droplets in host/pathogen interactions. Journal of Biological Chemistry **287:**2280-2287.
9. **D'Avila H, Freire-de-Lima CG, Roque NR, Teixeira L, Barja-Fidalgo C, Silva AR, Melo RC, Dosreis GA, Castro-Faria-Neto HC, Bozza PT.** 2011. Host cell lipid bodies triggered by *Trypanosoma cruzi* infection and enhanced by the uptake of apoptotic cells are associated with prostaglandin E(2) generation and increased parasite growth. Journal of Infectious Disease **204:**951-961.
10. **Pulido-Mendez M, Finol HJ, Giron ME, Aguilar I.** 2006. Ultrastructural pathological changes in mice kidney caused by *Plasmodium berghei* infection. Journal of Submicroscopic Cytology and Pathology **38:**143-148.
11. **Charron AJ, Sibley LD.** 2002. Host cells: mobilizable lipid resources for the intracellular parasite *Toxoplasma gondii*. Journal of Cell Science **115:**3049-3059.
12. **Lecoeur H, Giraud E, Prevost MC, Milon G, Lang T.** 2013. Reprogramming neutral lipid metabolism in mouse dendritic leucocytes hosting live *Leishmania amazonensis* amastigotes. PLoS Neglected Tropical Diseases **7:**e2276.
13. **Rabhi S, Rabhi I, Trentin B, Piquemal D, Regnault B, Goyard S, Lang T, Descoteaux A, Enninga J, Guizani-Tabbane L.** 2016. Lipid Droplet Formation, Their Localization and Dynamics during *Leishmania major* Macrophage Infection. PLoS One **11:**e0148640.
14. **Kumar Y, Cocchiaro J, Valdivia RH.** 2006. The obligate intracellular pathogen *Chlamydia trachomatis* targets host lipid droplets. Current Biology **16:**1646-1651.
15. **Daniel J, Maamar H, Deb C, Sirakova TD, Kolattukudy PE.** 2011. *Mycobacterium tuberculosis* uses host triacylglycerol to accumulate lipid droplets and acquires a dormancy-like phenotype in lipid-loaded macrophages. PLoS Pathogens **7:**e1002093.
16. **D'Avila H, Melo RC, Parreira GG, Werneck-Barroso E, Castro-Faria-Neto HC, Bozza PT.** 2006. *Mycobacterium bovis* bacillus Calmette-Guerin induces TLR2-mediated formation of lipid bodies: intracellular domains for eicosanoid synthesis *in vivo*. Journal of Immunology **176:**3087-3097.
17. **D'Avila H, Roque NR, Cardoso RM, Castro-Faria-Neto HC, Melo RC, Bozza PT.** 2008. Neutrophils recruited to the site of *Mycobacterium bovis* BCG infection undergo apoptosis and modulate lipid body biogenesis and prostaglandin E production by macrophages. Cellular Microbiology **10:**2589-2604.
18. **Mattos KA, Lara FA, Oliveira VG, Rodrigues LS, D'Avila H, Melo RC, Manso PP, Sarno EN, Bozza PT, Pessolani MC.** 2011. Modulation of lipid droplets by

Mycobacterium leprae in Schwann cells: a putative mechanism for host lipid acquisition and bacterial survival in phagosomes. Cellular Microbiology **13:**259-273.

19. **Ogawa M, Fukasawa M, Satoh M, Hanada K, Saijo M, Uchiyama T, Ando S.** 2014. The intracellular pathogen *Orientia tsutsugamushi* responsible for scrub typhus induces lipid droplet formation in mouse fibroblasts. Microbes and Infection **16:**962-966.
20. **Nawabi P, Catron DM, Haldar K.** 2008. Esterification of cholesterol by a type III secretion effector during intracellular Salmonella infection. Molecular Microbiology **68:**173-185.
21. **Cocchiaro JL, Kumar Y, Fischer ER, Hackstadt T, Valdivia RH.** 2008. Cytoplasmic lipid droplets are translocated into the lumen of the *Chlamydia trachomatis* parasitophorous vacuole. PNAS **105:**9379-9384.
22. **Mattos KA, D'Avila H, Rodrigues LS, Oliveira VG, Sarno EN, Atella GC, Pereira GM, Bozza PT, Pessolani MC.** 2010. Lipid droplet formation in leprosy: Toll-like receptor-regulated organelles involved in eicosanoid formation and *Mycobacterium leprae* pathogenesis. Journal of Leukocyte Biology **87:**371-384.
23. **Toledo DA, Roque NR, Teixeira L, Milan-Garces EA, Carneiro AB, Almeida MR, Andrade GF, Martins JS, Pinho RR, Freire-de-Lima CG, Bozza PT, D'Avila H, Melo RC.** 2016. Lipid Body Organelles within the Parasite *Trypanosoma cruzi*: A Role for Intracellular Arachidonic Acid Metabolism. PLoS One **11:**e0160433.
24. **Araujo-Santos T, Rodriguez NE, Moura-Pontes S, Dixt UG, Abanades DR, Bozza PT, Wilson ME, Borges VM.** 2014. Role of prostaglandin F2alpha production in lipid bodies from *Leishmania infantum chagasi*: insights on virulence. Journal of Infectious Disease **210:**1951-1961.
25. **Melo RC, Weller PF.** 2016. Lipid droplets in leukocytes: Organelles linked to inflammatory responses. Experimental Cell Research **340:**193-197.
26. **Justis AV, Hansen B, Beare PA, King KB, Heinzen RA, Gilk SD.** 2016. Interactions between the *Coxiella burnetii* parasitophorous vacuole and the endoplasmic reticulum involve the host protein ORP1L. Cellular Microbiology doi:10.1111/cmi.12637.
27. **Martinez E, Allombert J, Cantet F, Lakhani A, Yandrapalli N, Neyret A, Norville IH, Favard C, Muriaux D, Bonazzi M.** 2016. *Coxiella burnetii* effector CvpB modulates phosphoinositide metabolism for optimal vacuole development. PNAS **113:**E3260-3269.
28. **Mahapatra S, Ayoubi P, Shaw EI.** 2010. *Coxiella burnetii* Nine Mile II proteins modulate gene expression of monocytic host cells during infection. BMC Microbiology **10:**244.
29. **Ren Q, Robertson SJ, Howe D, Barrows LF, Heinzen RA.** 2003. Comparative DNA microarray analysis of host cell transcriptional responses to infection by *Coxiella burnetii* or *Chlamydia trachomatis*. Annals of the New York Academy of Sciences **990:**701-713.
30. **Brouqui P, Dumler JS, Raoult D.** 1994. Immunohistologic demonstration of *Coxiella burnetii* in the valves of patients with Q fever endocarditis. The American Journal of Medicine **97:**451-458.
31. **Graham JG, MacDonald LJ, Hussain SK, Sharma UM, Kurten RC, Voth DE.** 2013. Virulent *Coxiella burnetii* pathotypes productively infect primary human alveolar macrophages. Cellular Microbiology **15:**1012-1025.

32. **McDonough JA, Newton HJ, Klum S, Swiss R, Agaisse H, Roy CR.** 2013. Host pathways important for *Coxiella burnetii* infection revealed by genome-wide RNA interference screening. MBio **4:**e00606-00612.
33. **Sandoz KM, Valiant WG, Eriksen SG, Hruby DE, Allen RD, 3rd, Rockey DD.** 2014. The broad-spectrum antiviral compound ST-669 restricts chlamydial inclusion development and bacterial growth and localizes to host cell lipid droplets within treated cells. Antimicrobial Agents and Chemotherapy **58:**3860-3866.
34. **Soltysiak KA, van Schaik EJ, Samuel JE.** 2015. Surfactant protein D binds to *Coxiella burnetii* and results in a decrease in interactions with murine alveolar macrophages. PLoS One **10:**e0136699.
35. **Newton HJ, McDonough JA, Roy CR.** 2013. Effector protein translocation by the *Coxiella burnetii* Dot/Icm type IV secretion system requires endocytic maturation of the pathogen-occupied vacuole. PLoS One **8:**e54566.
36. **Long AP, Manneschmidt AK, VerBrugge B, Dortch MR, Minkin SC, Prater KE, Biggerstaff JP, Dunlap JR, Dalhaimer P.** 2012. Lipid droplet *de novo* formation and fission are linked to the cell cycle in fission yeast. Traffic **13:**705-714.
37. **Paul A, Chang BH, Li L, Yechoor VK, Chan L.** 2008. Deficiency of adipose differentiation-related protein impairs foam cell formation and protects against atherosclerosis. Circulation Research **102:**1492-1501.
38. **Bozza PT, Payne JL, Morham SG, Langenbach R, Smithies O, Weller PF.** 1996. Leukocyte lipid body formation and eicosanoid generation: cyclooxygenase-independent inhibition by aspirin. PNAS **93:**11091-11096.
39. **Vieira-de-Abreu A, Calheiros AS, Mesquita-Santos FP, Magalhaes ES, Mourao-Sa D, Castro-Faria-Neto HC, Bozza MT, Bandeira-Melo C, Bozza PT.** 2011. Cross-talk between macrophage migration inhibitory factor and eotaxin in allergic eosinophil activation forms leukotriene C(4)-synthesizing lipid bodies. American Journal of Respiratory Cell and Molecular Biology **44:**509-516.
40. **Igal RA, Wang P, Coleman RA.** 1997. Triacsin C blocks *de novo* synthesis of glycerolipids and cholesterol esters but not recycling of fatty acid into phospholipid: evidence for functionally separate pools of acyl-CoA. The Biochemical Journal **324 (Pt 2):**529-534.
41. **Cao J, Zhou Y, Peng H, Huang X, Stahler S, Suri V, Qadri A, Gareski T, Jones J, Hahm S, Perreault M, McKew J, Shi M, Xu X, Tobin JF, Gimeno RE.** 2011. Targeting Acyl-CoA:diacylglycerol acyltransferase 1 (DGAT1) with small molecule inhibitors for the treatment of metabolic diseases. The Journal of Biological Chemistry **286:**41838-41851.
42. **Mayer N, Schweiger M, Romauch M, Grabner GF, Eichmann TO, Fuchs E, Ivkovic J, Heier C, Mrak I, Lass A, Hofler G, Fledelius C, Zechner R, Zimmermann R, Breinbauer R.** 2013. Development of small-molecule inhibitors targeting adipose triglyceride lipase. Nature Chemical Biology **9:**785-787.
43. **Deb C, Daniel J, Sirakova TD, Abomoelak B, Dubey VS, Kolattukudy PE.** 2006. A novel lipase belonging to the hormone-sensitive lipase family induced under starvation to utilize stored triacylglycerol in *Mycobacterium tuberculosis*. The Journal of Biological Chemistry **281:**3866-3875.
44. **Dvorak AM, Dvorak HF, Peters SP, Shulman ES, MacGlashan DW, Jr., Pyne K, Harvey VS, Galli SJ, Lichtenstein LM.** 1983. Lipid bodies: cytoplasmic organelles

565 important to arachidonate metabolism in macrophages and mast cells. Journal of
566 Immunology **131:**2965-2976.
567 45. **Weller PF, Monahan-Earley RA, Dvorak HF, Dvorak AM.** 1991. Cytoplasmic lipid
568 bodies of human eosinophils. Subcellular isolation and analysis of arachidonate
569 incorporation. The American Journal of Pathology **138:**141-148.
570 46. **Mattos KA, Oliveira VG, D'Avila H, Rodrigues LS, Pinheiro RO, Sarno EN,**
571 **Pessolani MC, Bozza PT.** 2011. TLR6-driven lipid droplets in *Mycobacterium leprae*-
572 infected Schwann cells: immunoinflammatory platforms associated with bacterial
573 persistence. Journal of Immunology **187:**2548-2558.
574 47. **Koster FT, Williams JC, Goodwin JS.** 1985. Cellular immunity in Q fever: modulation
575 of responsiveness by a suppressor T cell-monocyte circuit. Journal of Immunology
576 **135:**1067-1072.
577 48. **Izzo AA, Marmion BP.** 1993. Variation in interferon-gamma responses to *Coxiella*
578 *burnetii* antigens with lymphocytes from vaccinated or naturally infected subjects.
579 Clinical and Experimental Immunology **94:**507-515.
580 49. **Cockrell DC, Beare PA, Fischer ER, Howe D, Heinzen RA.** 2008. A method for
581 purifying obligate intracellular *Coxiella burnetii* that employs digitonin lysis of host cells.
582 Journal of Microbiological Methods **72:**321-325.
583 50. **Beare PA, Gilk SD, Larson CL, Hill J, Stead CM, Omsland A, Cockrell DC, Howe**
584 **D, Voth DE, Heinzen RA.** 2011. Dot/Icm type IVB secretion system requirements for
585 *Coxiella burnetii* growth in human macrophages. MBio **2:**e00175-00111.
586 51. **Omsland A, Cockrell DC, Howe D, Fischer ER, Virtaneva K, Sturdevant DE,**
587 **Porcella SF, Heinzen RA.** 2009. Host cell-free growth of the Q fever bacterium *Coxiella*
588 *burnetii*. PNAS **106:**4430-4434.
589 52. **Sanjana NE, Shalem O, Zhang F.** 2014. Improved vectors and genome-wide libraries
590 for CRISPR screening. Nature Methods **11:**783-784.
591 53. **Coleman SA, Fischer ER, Howe D, Mead DJ, Heinzen RA.** 2004. Temporal analysis
592 of *Coxiella burnetii* morphological differentiation. The Journal of Bacteriology
593 **186:**7344-7352.
594

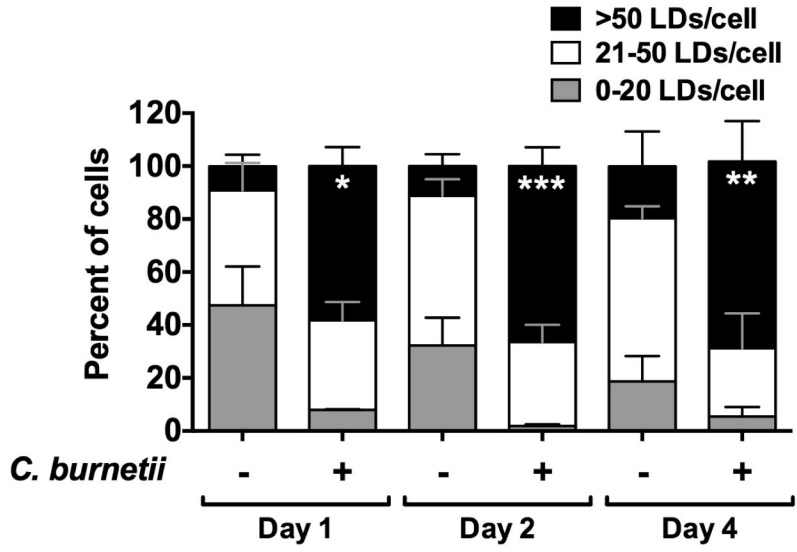

Figure 1: *C. burnetii* infection results in host cell LD accumulation.
MH-S macrophages were infected with *C. burnetii* NMII and at different times post-infection, cells were stained for PLIN2 (LDs), LAMP1 (PV marker) and *C. burnetii*. LDs were observed by fluorescence microscopy and number of LDs per cell was quantitated. The percent of counted cells containing 0-20, 21-50 and >50 LDs per cell at respective times were plotted. Error bars show the mean of 3 independent experiments +/- SEM * =$p<0.05$, ** =$p<0.01$, *** =$p<0.001$ compared to respective >50 LDs/cell in mock-infected cells as determined by two-way ANOVA with Tukey post-hoc test.

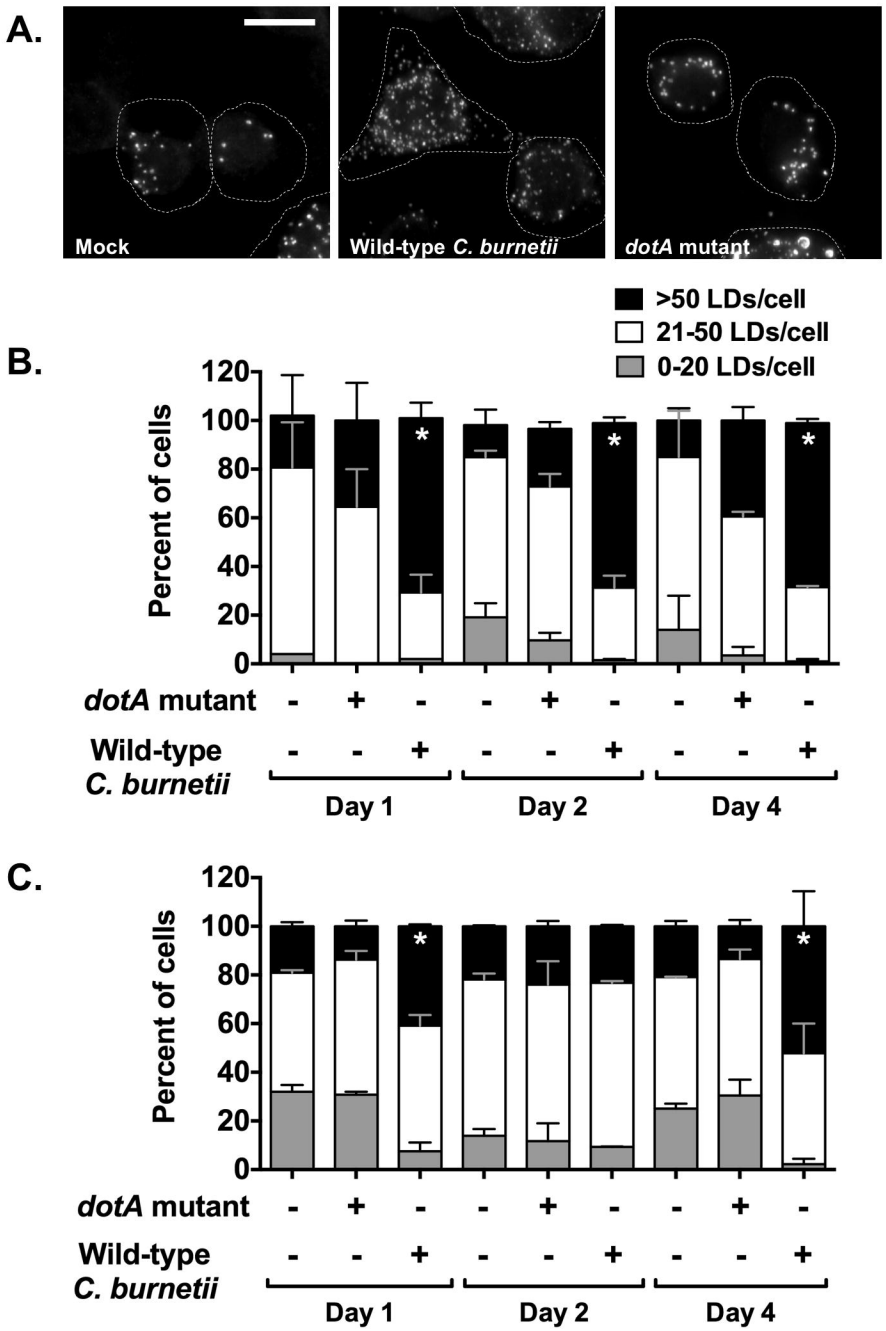

Figure 2: Host cell LD accumulation is dependent on the *C. burnetii* T4BSS Secretion System (T4BSS).

A) Representative images of mock, wild-type *C. burnetii* NMII and T4BSS *(dotA)* mutant-infected MH-S macrophages stained for PLIN2 (LDs) at day 1 post-infection imaged at 100X. Scale bar = 10 μm

B) MH-S macrophages and (C) THP-1 monocyte-derived macrophages were infected with wild-type *C. burnetii* NMII and *dotA* mutant. At different time points post-infection, cells were stained for PLIN2 (LDs), LAMP1 (PV marker) and *C. burnetii*. The number of LDs per cell were counted by fluorescence microscopy. Percent of cells containing 0-20, 21-50 and >50 LDs per cell at respective time points were plotted. Error bars show the mean of 3 independent experiments +/- SEM * =$p<0.05$ compared to respective >50 LDs/cell in *dotA* mutant-infected cells as determined by two-way ANOVA with Tukey post-hoc test.

Figure 3: Blocking LD formation increases *C. burnetii* growth.

C. burnetii NMII growth in infected MH-S cells treated with different inhibitors was measured at 2 and 4 days post-infection by FFU assay.

A) Representative images for wild-type MH-S macrophages treated with inhibitors, fixed, stained for PLIN2 (LDs) and imaged day 1 post-treatment at 100X. Scale bar = 10 μm

B) Growth in LD formation inhibitor triascin C–treated (10 μM) wild-type MH-S macrophages. Error bars represent the mean of 4 independent experiments +/- SEM. **= $p < 0.01$ compared to vehicle treated cells as determined by two-way ANOVA with Bonferroni post-hoc test.

C) ACAT1 protein expression in wild-type and *acat-1*$^{-/-}$ macrophages. Cell lysates were immunoblotted and ACAT1 protein levels were compared with GAPDH as loading control.

D) Representative images for vehicle-treated wild-type MH-S macrophages and vehicle and T863-treated *acat-1*$^{-/-}$ macrophages fixed, stained for PLIN2 (LDs) and imaged day 1 post-treatment at 100X. Scale bar = 10 μm

E) *C. burnetii* NMII growth in vehicle-treated wild-type and *acat-1*$^{-/-}$ MH-S macrophages and (F) T863-treated wild-type and *acat-1*$^{-/-}$ MH-S macrophages. Error bars represent the mean of 3 independent experiments +/- SEM., * =$p<0.05$, *** =$p < 0.001$ as determined by two-way ANOVA with Bonferroni post-hoc test.

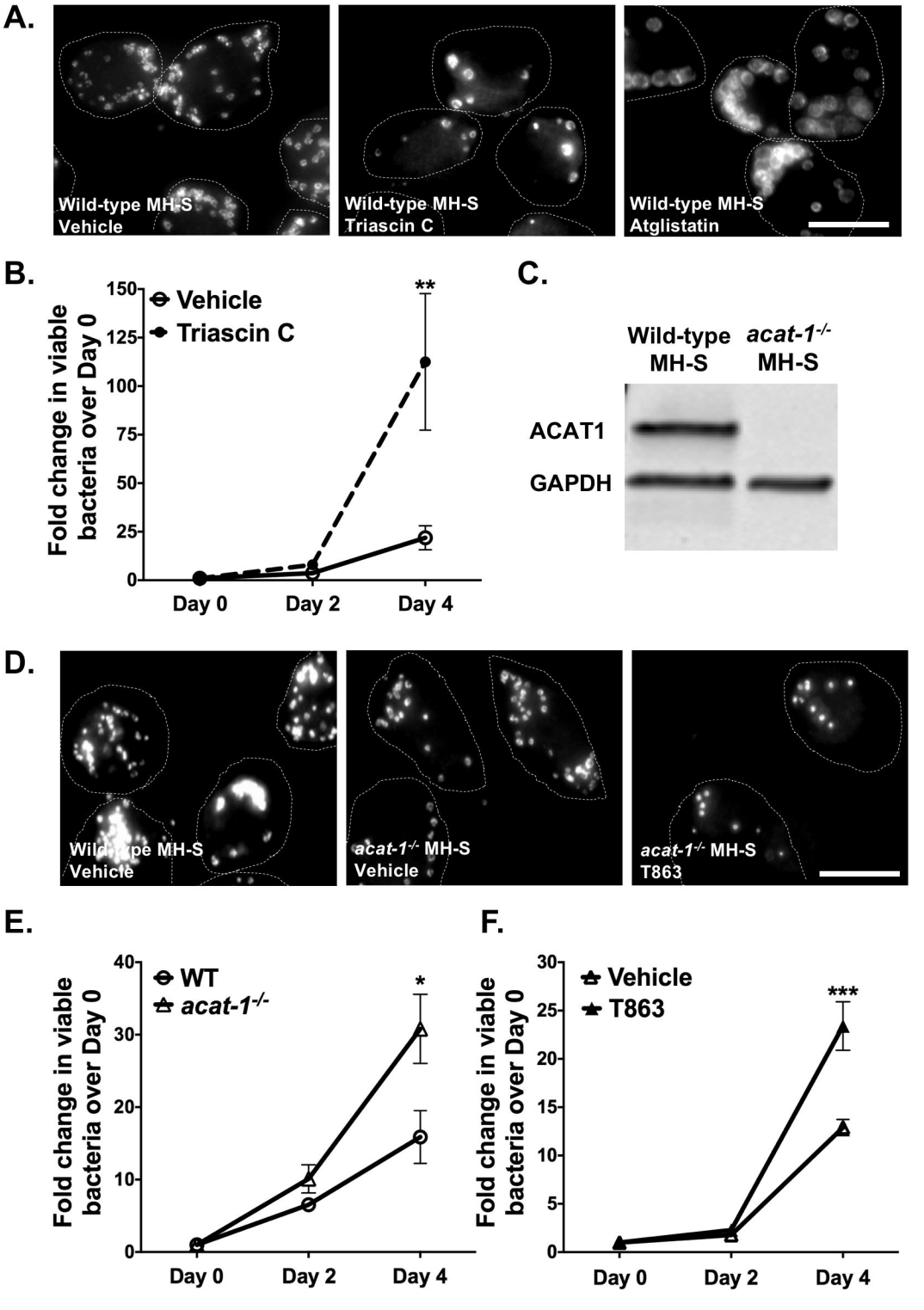
A.
Wild-type MH-S
Vehicle
Wild-type MH-S
Triascin C
Wild-type MH-S
Atglistatin
B.
Vehicle
Triascin C
Fold change in viable bacteria over Day 0
150
125
100
75
50
25
0
**
Day 0
Day 2
Day 4
C.
Wild-type MH-S
acat-1-/- MH-S
ACAT1
GAPDH
D.
Wild-type MH-S
Vehicle
acat-1-/- MH-S
Vehicle
acat-1-/- MH-S
T863
E.
WT
acat-1-/-
Fold change in viable bacteria over Day 0
40
30
20
10
0
*
Day 0
Day 2
Day 4
F.
Vehicle
T863
Fold change in viable bacteria over Day 0
30
25
20
15
10
5
0
***
Day 0
Day 2
Day 4

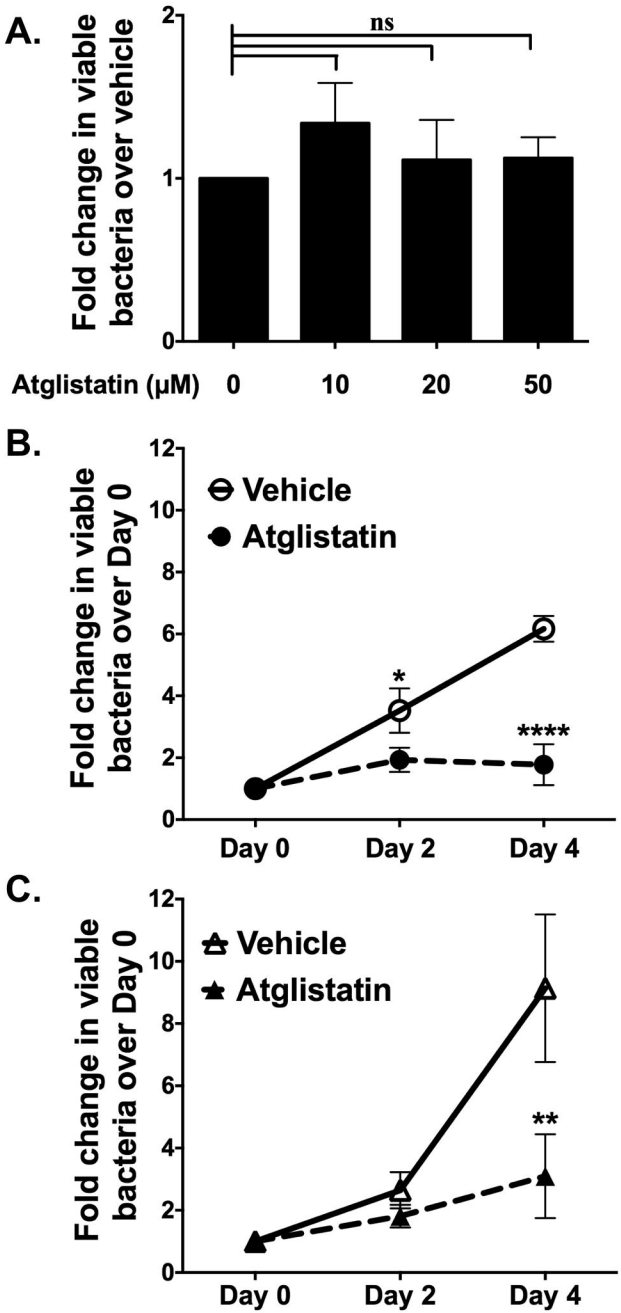

Figure 4: Inhibiting LD breakdown blocks *C. burnetii* growth.

Effect of ATGL inhibitor atglistatin on viability of axenic and intracellular *C. burnetii* NMII was determined by FFU assay.

A) Direct effect of atglistatin on *C. burnetii* NMII. Atglistatin was added to axenic *C. burnetii* cultures and bacterial viability was determined at day 4 using FFU assay. Error bars represent the mean of 3 independent experiments +/- SEM. ns = not significant compared to vehicle treatment as determined by ordinary one-way ANOVA with Tukey post-hoc test.

B) Growth in atglistatin-treated (20 μM) and vehicle-treated wild-type MH-S macrophages. Error bars represent the mean of 4 independent experiments +/- SEM. *= $p < 0.05$, **** =$p<0.0001$ compared to vehicle-treated cells as determined by two-way ANOVA with Bonferroni post-hoc test.

C) Growth in atglistatin-treated (20 μM) and vehicle-treated *acat-1*$^{-/-}$ MH-S macrophages. Error bars represent the mean of 4 independent experiments +/- SEM. ** =$p<0.01$ compared to vehicle treated cells as determined by two-way ANOVA with Bonferroni post-hoc test.